Antibody Therapeutics, 2025, 8(1), 26–39
https://doi.org/10.1093/abt/tbae031
Advance access publication date 16 December 2024
Research Article

Humanized anti-CD11d monoclonal antibodies suitable for basic research and therapeutic applications

Eoin N. Blythe[1], Christy Barreira[2], Corby Fink[1], Arthur Brown[3], Lynne C. Weaver[4], Gregory A. Dekaban[1,*]

[1]Department of Microbiology & Immunology and Robarts Research Institute, University of Western Ontario, London, Ontario N6A 5B7, Canada
[2]Robarts Research Institute, University of Western Ontario, London, Ontario N6A 5B7, Canada
[3]Department of Anatomy & Cell Biology and Robarts Research Institute University of Western Ontario, London, Ontario N6A 5B7, Canada
[4]Department of Physiology & Pharmacology and Robarts Research Institute, University of Western Ontario, London, Ontario N6A 5B7, Canada

[*]Corresponding author. Department of Microbiology and Immunology, Dental Sciences Building, Rm2014, University of Western Ontario, 1151 Richmond Street North, London, Ontario N6A 5B7, Canada. E-mail: dekaban@uwo.ca

Abstract

Background: Immunomodulatory agents targeting the CD11d/CD18 integrin are in development for the treatment of several pathophysiologies including neurotrauma, sepsis, and atherosclerosis. Murine anti-human CD11d therapeutic antibodies have successfully improved neurological and behavioral recovery in rodent neurotrauma models. Here, we present the progression of CD11d-targeted agents with the development of humanized anti-CD11d monoclonal antibodies.
Methods: Primary human leukocytes and the THP-1 monocytic cell line were used to determine the binding of the CD11d antibodies, determine binding affinities, and assess outside-in signaling induced by CD11d antibody binding. In addition, a rat model of spinal cord injury was employed to demonstrate that the humanized monoclonal antibodies retained their therapeutic function *in vivo*. These determinations were made using a combination of flow cytometry, western blotting, immunohistochemistry, biochemical assays, and a locomotor behavioral assessment.
Results: Flow cytometric analysis demonstrated that the humanized anti-CD11d clones bind both human monocytes and neutrophils. Using a THP-1 model, the humanized anti-CD11d-2 clone was then determined to bind both the active and inactive CD11d/CD18 conformations without inducing inflammatory cell signaling. Finally, an investigation using anti-CD11d-2 as a detection tool uncovered a mismatch between total and surface-level CD11d and CD18 expression that was not altered by CK2 inhibition.
Conclusions: By developing humanized anti-CD11d monoclonal antibodies, new tools are now available to study CD11d biology and potentially treat inflammation arising from acute neurotrauma via CD11d targeting.

Statement of Significance:
We describe the first humanized monoclonal antibodies to the β2 integrin CD11d alpha chain. These antibodies bind to CD11d on primary human leukocytes and the anti-CD11d-2 clone did not induce outside-in signaling. The screened humanized anti-CD11d clones recapitulate the ability of the mouse parental anti-CD11d to improve neurological outcomes in a rat acute neurotrauma model.

Keywords: integrin; monoclonal antibody; CD11dCD18; therapeutic antibody

Introduction

Integrins are adhesion molecules involved in the recruitment and retention of leukocytes during an inflammatory response. CD11d/CD18 is a β2 integrin that promotes extravasation of leukocytes via binding to human vascular adhesion molecule 1 (VCAM-1) and intracellular adhesion molecule 3 (ICAM-3) while also contributing to tissue migration via binding to an array of extracellular matrix ligands [1]. Developing novel immunomodulatory therapeutics against CD11d/CD18 is a subject of current interest. Our laboratory has pursued anti-CD11d therapeutic antibodies [2–5], while other laboratories have pursued small peptide inhibitors [6]. The common goal of CD11d-targeted therapeutic agents is to disrupt the accumulation of pro-inflammatory leukocytes within target tissues [1].

A perceived benefit of CD11d-targeted therapies is the low and limited expression of CD11d/CD18 that is subsequently increased during select pathophysiologies [1]. Damaging accumulation of neutrophils and monocytes is linked to the upregulation of CD11d/CD18 on these leukocytes during the acute stages of neurotrauma [7] and respiratory distress syndrome [8, 9]. Chronic accumulation of pro-inflammatory macrophages has been associated with increased levels of CD11d in atherosclerosis [10], obesity [11], and nonalcoholic steatohepatitis [12, 13]. Past work has detailed the genetic regulation of the CD11d gene [14–17], but less is known regarding the post-transcriptional regulation and subsequent cell surface expression of the CD11d protein [18].

Historically, integrin-targeted immunotherapies have been limited by their broad impacts that lead to serious side effects. Efalizumab was an early integrin-targeted immunotherapy that targeted the CD11a/CD18 β2 integrin expressed on all leukocytes. Blockage of CD11a/CD18 with efalizumab resulted in broad

Received: September 19, 2024. **Revised:** November 20, 2024. **Accepted:** December 13, 2024

immunosuppression and reactivation of the john cunningham (JC) virus [19]. Modern approaches to integrin-targeted immunotherapies have addressed the broad immunosuppression problem by targeting integrins with restricted expression profiles. Vedolizumab was designed against the $\alpha 4\beta 7$ integrin, which is primarily restricted to leukocyte recruitment within the gastrointestinal tract [20, 21]. Clinical use of vedolizumab resulted in effective treatment of inflammatory bowel disease (Crohn's and ulcerative colitis) without prohibitive adverse events [22, 23]. The regulated expression profile of CD11d likewise provides an avenue to treat pathology with minimal systemic effects. Understanding the potential side effects of CD11d-targeted agents, however, cannot be determined by CD11d-expression profiles alone. Elucidating whether a CD11d-targeted agent binds the active and/or inactive conformations of CD11d/CD18 and whether it may induce or inhibit inflammatory cell signaling are important considerations.

Previously, our laboratory has demonstrated that a mouse anti-human CD11d clone (217 L) improves behavioral and neurological recovery within rodent neurotrauma models [2–5] as well as demonstrating the mechanistic consequences of anti-CD11 treatment that contributed to the neurological benefits obtained [24–33]. In the following report, we showcase an array of humanized anti-CD11d clones that can be used as a new tool in studying CD11d/CD18 mechanics. Among the humanized anti-CD11d clones, we identified a potential therapeutic clone (anti-CD11d-2) and characterized its binding dynamics. Finally, we uncovered an unexpected phenomenon of $\beta 2$ integrin downregulation with a maintained mismatch between total vs surface level CD11d expression following the blockade of CK2 phosphorylation in PMA differentiated THP-1 cells.

Materials and methods

The studies reported were conducted in a manner consistent with animal research: reporting of in vivo experiments (ARRIVE) guidelines.

CD11d humanized monoclonal antibody derivation

The original 217 L mouse anti-human CD11d clone, provided by Eli Lily & Co [34], was used as the basis for creating humanized monoclonal anti-CD11d antibodies. Complementarity-determining regions (CDRs) of the original 217 L clone were isolated, and four subsequent CDR variants were produced. The five resulting CDR sequences were incorporated into a human IgG4 framework to create the final clones (United States Patent No. US-11873340-B2 January 16, 2024) [35]. Specificity was verified by flow cytometry using HEK293 cells transfected with expression vectors expressing human CD11d and CD18 in the absence of any other $\beta 2$ integrin. The purified humanized CD11d monoclonal antibodies (anti-CD11d-1, anti-CD11d-2, anti-CD11d-3, anti-CD11d-4, anti-CD11d-5) were initially provided by Eli Lily & Co. Subsequently, the humanized CD11d monoclonal antibodies were produced in chinese hamster ovary (CHO) cells and then purified from culture supernatants under contract with Biologics at the Human Health Therapeutics Research Center, National Research Council Canada, Montreal, Canada. Endotoxin levels were determined to be <0.1 EU/mg.

Human leukocyte collection

Acquiring human blood samples for this study was approved (Project ID: 7332) by the University of Western Ontario Health Science Ethics Review Board (HSERB). After obtaining informed consent, human peripheral blood was collected via venipuncture in heparin vacutainer tubes (BD, San Jose, CA, USA) as approved by the HSERB and in accordance with an approved Biosafety-Biohazard Protocol (BIO-RRI-0021).

Cell culture

THP-1 (ATCC TIB-202) and THP-1 NF-kB-Luc2 (ATCC TIB-202-NFkB-Luc2) and Jurkat T cells were all obtained from American Tissue Culture Collection (ATCC, Cedarlane). All cells were cultured with complete Roswell park memorial institute (RPMI) media supplemented with 10% FBS, 1% L-glutamine, 100 U/ml penicillin, 100 μg/ml streptomycin, 1 mM sodium pyruvate, 10 nM (4-(2-hydroxyethyl)-1-piperazineethanesulphonic acid) (HEPES), and 50 μM 2-mercaptoethanol. Additionally, 1 μg/ml of puromycin was added to the complete RPMI selection media for the THP-1 NF-kB-Luc2 cell line. All tissue culture media, plastic ware, and supplements were acquired from ThermoFisher Scientific. Jurkat T cell cultures were grown in standing T75 flasks at 37°C and 5% CO_2 in a humidified incubator, and cell density did not exceed 1×10^6 cells/ml. THP-1 cells were seeded at 1×10^6 cells/well into 6-well plates, 2×10^5 cells/well into 12-well plates, or 6×10^4 cells/well into 96-well plates and differentiated with 100 nM of phorbol myristic acetate (PMA; Millipore Sigma), for up to 72 h.

Flow cytometry

Rat and human primary whole blood leukocytes were stained for flow cytometry as previously described [36]. THP-1 cells were either differentiated or cultured as previously described. A 15-min incubation at 37°C and 5% CO_2 with 1 ml Versene (ThermoFisher Scientific) was used to collect adherent cells following differentiation. To block promiscuous antibody binding, THP-1 cells were resuspended in 200 μl Hank's balanced salt solution (HBSS) + 0.1% bovine serum albumin (BSA) plus 5 μl normal goat serum (Jackson ImmunoResearch) and 5 μl AB human serum (ThermoFisher Scientific) on ice for 20 min. Cells were then surface-stained in fluorescent activated cell sorting (FACS) tubes (Corning) with a combination of LIVE/DEAD Fixable Aqua Dead Cell Stain Kit (ThermoFisher Scientific), anti-CD18 (TS1/18) fluorescein (FITC) (BioLegend), anti-CD11d (anti-CD11d-2) Alexa 647, anti-IgG4 Alexa 647 (Eli Lily & Co), anti-CD11a (TS2/4) PerCP (BioLegend), anti-CD11b (ICRF44) Violet 421 (BioLegend), and/or anti-CD11c (3.9) PE-Cy7 (BioLegend).

Intracellular staining was performed in a 96-well U-bottom plate (Corning) after performing fixable vital dye and/or cell surface staining. Cells were washed in staining buffer (HBSS + 0.1% BSA) and then fixed and permeabilized using the manufacturer's instructions (Foxp3/Transcription Factor Staining Buffer Set, eBioscience, ThermoFisher Scientific). The cells were then spun down, and each well was resuspended in a 50 μl permeabilization buffer containing BioLegend TruStain human FcX block and incubated for 5–10 min at room temperature. Without washing, cells were stained with all intracellular antibodies or isotype control antibodies for 20 min at room temperature. This was followed by two washes in 200 μl of permeabilization buffer and two washes in 200 μl of HBSS + 0.1% BSA. Cells were then resuspended in HBSS + 0.1% BSA followed by an appropriate amount of 4% paraformaldehyde (PFA) (BioShop) to allow for a final concentration of 1% PFA in each well.

For saturated antibody binding curves to determine antibody affinity, blocking and surface staining occurred live in HBSS, HBSS + 1 mM ethylenediaminetetraacetic acid (EDTA), or HBSS + 1 mM Mn^{2+}, and flow cytometry was performed on cells that were subsequently fixed.

For CK2 inhibition, the SGC-CK2–1 inhibitor was a gift from Dr. David Litchfield (Western University, Canada) and can be found commercially at MedKoo Biosciences. THP-1 cells were treated with or without 5 μM of SGC-CK2-1 in the presence or absence of 100 nM PMA for 48 h. Cells were fixed and stained as described above. Flow cytometry graphs of a 48-h dimethyl sulfoxide (DMSO) control treatment can be found in Supplemental Fig. 1B.

A BD LSR II flow cytometer (BD Biosciences) was used for data acquisition with at least 50 000 total cells recorded per experimental condition. Data were analyzed on FlowJo, version 10.8 (BD Life Sciences) [37]. Gating strategies can be found in Supplemental Fig. 2.

Experimental spinal cord injury and anti-CD11d anti-inflammatory treatment

All animal experiments were approved by the University of Western Ontario's Animal Care Committee (AUP no. 2010-237) and conducted in accordance with the Canadian Council of Animal Care guidelines, the University Animal Care Committee's Standard Operating Procedures, and the University's Biosafety-Biohazard Protocol (BIO-RRI-0021). Additionally, all animal experiments were conducted in accordance with the Standards for Humane Care and Use of Laboratory Animals as approved by the Office of Laboratory Animal Welfare, Department of Health & Human Services, U.S.A. (Protocol Assurance Identification #A5527-01).

Experimental spinal cord injury (SCI) was induced at the T4 spinal cord segment in female 220 g Wistar rats (Charles River). The T4 spinal cord segment was exposed by a dorsal laminectomy and injured, without disrupting the dura by a 60 second clip compression using a 50 g clip as previously described [2, 38] and randomly assigned to a treatment group. Postoperative care was provided as described previously [38]. To measure neutrophil infiltration into the spinal lesion using a myeloperoxidase assay, rats were given anti-CD11d clones at 2 h post-SCI for the 24-h assay time point, or at 2, 24, and 48 h post-SCI for the 72-h assay time point, as previously described [25]. For rats undergoing open-field locomotor assessment, the anti-CD11d clone was administered intravenously via the tail vein at 2, 24, and 48 h post-SCI. All animals were monitored twice daily using a veterinarian-approved clinical scoring sheet that monitored the level of alertness and activity, hydration status (water consumption), percent weight loss, appearance of the surgical wound, evidence of pain (piloerection, hunched back, discoloration around eyes), bowel movements (presence of fecal pellets in cage), bladder fullness, urine leakage, and appearance (cloudy, presence of blood). Bladders were emptied twice per day by gentle manual compression.

Basso, Beattie, and Bresnahan rat open-field locomotor assessment

Hind limb locomotor assessment was conducted using the Basso, Beattie, and Bresnahan (BBB) locomotor rating scale for open-field testing, as previously described [2, 39]. Testing was done twice per week, and scores were averaged to generate a weekly score. Scores of left and right legs were averaged. The BBB assessment was conducted by four individuals experienced in the BBB open-field locomotor assessment and who were blinded to the treatment each rat received until after the end of the 10-week assessment.

Myeloperoxidase assay

At the 24 and 72 h time points, spinal cord–injured rats were euthanized by deep induction of anesthesia with 4% isoflurane followed by exsanguination (cardiac perfusion with cold phosphate buffered saline [PBS]). Spinal cord tissue was harvested around the lesion, and a homogenate was prepared as previously described [2]. A portion of the homogenates was then assayed for myeloperoxidase activity as a surrogate marker for the presence of neutrophils. Complete methods of the myeloperoxidase assay were performed as previously described [25].

Immunocytochemistry

THP-1 NF-kB-Luc2 cells were seeded onto circular cover glasses placed at the bottom of 12-well plates and differentiated with RPMI selection media containing 100 nM of PMA for 48 h at 37°C and 5% CO_2. RPMI selection media were removed, and cells were washed once with HBSS + 0.1% BSA. In 300 μl of HBSS + 0.1%, cells were blocked with 15 μl of FcX TruStain block (BioLegend) for 20 min at 10°C. The remainder of the staining procedure occurred at room temperature in the dark. In 500 μl of fresh HBSS, anti-CD11d (anti-CD11d-2) Alexa-647 (3 μg/ml) and anti-CD18 (TS1/18) FITC (10 μg/ml) were applied for 20 min. Cells were washed once with HBSS and fixed in 4% PFA for 20 min. Following three washes with 1 ml of HBSS, cells were permeabilized with 0.1% Triton X in HBSS for 15 min. In 300 μl of HBSS, 1:1000 DAPI stain (Millipore Sigma) was applied for 20 min. Finally, cells were washed three times with 1 ml of HBSS, and imaging was performed on a Leica DMI6000 microscope (Leica Microsystems) and an electron multiplication charged-coupled device (EM CCO) EvOLVE camera (Teledyne Photometrics). Images were analyzed on the FIJI software platform [40].

Western blot

THP-1 cells were differentiated or cultured in a 6-well plate as previously described in cell culture methods. Next, the culture media were removed, and the cells were washed twice with 1 ml PBS. The cells were incubated in 1 ml of ethylene glycol-bis(β-aminoethyl ether)-N,N,N′,N′-tetraacetic acid (EGTA) -supplemented PBS for 15 min at 37°C and 5% CO_2, to minimize focal adhesion signaling. Cells were washed twice with 1 ml PBS and then stimulated in 1 ml of complete RMPI media at 37°C and 5% CO_2. Following stimulation, cells were immediately washed in 1 ml of ice-cold PBS and lysed with radioimmunoprecipitation assay (radioimmunoprecipitation assay [RIPA] buffer) containing Halt Protease and Halt Phosphatase inhibitor cocktails (ThermoFisher Scientific). A cell scraper was used to collect cell lysate from adherent differentiated cells, and nonadherent undifferentiated cells were collected directly into Eppendorf tubes. Lysates were placed on ice for 15 min and then sonicated twice for 10 s for complete lysis. A Bradford assay determined protein concentrations using detergent-compatible protein assay reagents (Bio-Rad Laboratories). The resulting supernatants were immediately stored at −80°C.

For gel electrophoresis, lysate samples were mixed in 2× Tris-glycine buffer (BioLegend). Premade Tris-glycine gels (10%) (ThermoFisher Scientific) were loaded with 40 μl of sample or 3 μl of BLUeye protein ladder (FroggaBio). The gels were run for 150 min at 125 V and then transferred for 60 min at 100 V onto Immobilon PVDF (Bio-Rad Laboratories). In fresh 5 ml of Tris buffered saline (TBS) intercept blocking buffer (Li-Cor), cells were incubated overnight at 4°C with mouse anti-phosphotyrosine (PY20) (BioLegend) and rabbit Focal Adhesion Kinase (FAK) protein (3285) (Cell Signaling Technology). Membranes were washed three times with 5 ml TBS + 0.1% Tween 20 (BioShop) for 5 min. In fresh 5 ml of TBS intercept blocking buffer, secondary donkey anti-rabbit 680RD and donkey antimouse 800CW (Li-Cor) were incubated at room temperature for 1 h. Membranes were imaged at 700 and

800 nm using an Odyssey Fc (Li-Cor). Blots were then stripped and reprobed overnight with rabbit anti-pTyr397 FAK (700255) (ThermoFisher Scientific) and mouse β-actin mouse (A2228) (Sigma Aldrich). Data were analyzed on Image Studio Lite, version 5.2 (Li-Cor). Raw blots can be found in Supplemental Fig. 3.

For detection of CK2 phosphorylation, undifferentiated THP-1 cells were treated with 5 μM SGC-CK2-1 inhibitor for 12, 24, or 48 h. Cell lysates were collected, and gel electrophoresis occurred as described above. CK2 phosphorylation was detected by rabbit EIF2S2-pS2 [41] (gifted by Dr David Litchfield, University of Western Ontario, London, ON, Canada) and normalized to mouse β-actin (A2228) expression. Secondary antibodies and imaging occurred as described above.

Bioluminescence

THP-1 NF-kB-Luc2 cells were seeded at 6×10^4 cells/well of an opaque flat 96-well plate (Corning) in 100 μl of RMPI complete media. Selected plates were differentiated with 100 nM PMA for 48 h, washed once with HBSS, and then rested in serum-free RPMI complete selection media for 24 h. Next, all the media were removed, replaced with 100 μl of RMPI complete media containing 150 μg/ml D-luciferin (Syd Labs), and treated with various conditions. The undifferentiated plates were immediately treated with 150 μg/ml D-luciferin and various conditions. Plates were incubated in a Cytation 5 imager (Agilent Technologies) at 37°C and 5% CO_2 for 24 h, and bioluminescence was read every hour for 24 h.

CD11d structure modeling

The computational CD11d structure (AF-Q13349-F1-v4) was downloaded from the AlphaFold Creative Commons archive [42, 43]. PyMOL software (Molecular Graphics System, Version 3.0 Schrödinger, LLC.) was then used to visualize the predicted CD11d tertiary structure, and the I-domain (residues 148–336) was isolated. Finally, the adaptive poisson-boltzmann solver (APBS) electrostatics PyMOL plugin was used to visualize the surface distribution of electrostatic charges.

Statistical analysis

Statistical analyses were performed using GibStat or GraphPad Prism, Version 9. All data were presented as the mean plus/minus the standard error of the mean. Statistical significance was detected at $P < .05$. Biological replicates were denoted by *N*, whereas technical replicates were denoted by *n*. One-way and two-way ANOVAs were performed with appropriate *post hoc* tests for multiple comparisons as noted in the figure legends.

Results

Creation of humanized anti-CD11d clones

Initial anti-CD11d therapeutic antibodies were obtained from mice and tested as a treatment for acute SCI by modulating the migration of leukocytes into the lesion area. An original murine 217 L monoclonal antibody was produced that targeted the ligand-binding α-I domain of human CD11d. The murine 217 L clone bound both human and rat CD11d-expressing leukocytes [34]. In rodent trials of SCI, rats treated with 217 L anti-CD11d had significantly improved biochemical and behavioral recoveries [2]. A humanized anti-CD11d therapeutic clone (anti-CD11d-1) was created by combining the CDR of the murine 217 L clone and the scaffolding of a human IgG4 framework. Additionally, four variants of the murine 217 L CDR sequence (anti-CD11d-2, anti-CD11d-3, anti-CD11d-4, anti-CD11d-5) were produced and subsequently combined with the same human IgG4 framework. In total, five humanized IgG4 antibodies targeting human CD11d were produced and verified for specificity [18, 35] (Fig. 1A). The performance of the humanized anti-CD11d clones on human blood samples was tested by flow cytometry. The anti-CD11d-2 clone bound human monocytes and neutrophils at the greatest percentage and mean fluorescence intensity (MFI; Fig. 1B–E). The humanized anti-CD11d clones compare well with historical data of the original 217 L clone (mouse anti-human CD11d mAb) binding to human leukocytes as described previously by Bao *et al.* [7]. The anti-CD11d 1–5 clones and the IgG4 isotype control exhibited the same minimal nonspecific binding to Jurkat T cells that do not express CD11d (Fig. 1F) as T cells positive for the $\alpha\beta$ T-cell receptor do not express CD11d [44]. Subsequently, anti-CD11d-2 was used to identify the expression levels of CD11d among monocyte subsets. The nonclassical $CD14^+$ $CD16^+$ monocytes exhibited the highest level of surfaced expressed CD11d as reflected by having the greatest MFI among the three defined subsets (Fig. 1G and H).

Functional screen of humanized anti-CD11d clones in a neurotrauma rat model

We have previously published extensive research on the performance of murine antihuman (217 L) and hamster anti-mouse CD11d clones (205C) in multiple neurotrauma rodent models [2–5]. The previously published articles demonstrated that anti-CD11d reduced leukocyte infiltration into the central nervous system (CNS) by histological detection, myeloperoxidase (MPO) assay neutrophil detection, and ED-1 western blot macrophage detection [2–5]. Additionally, anti-CD11d treatment increased myelin sparing post-injury [2, 3, 5] and improved locomotor recovery [2, 3, 5]. Mechanistically, these anti-CD11d-driven improvements in recovery can be explained by a reduction in the presence of free radicals in the CNS and a subsequent reduction in oxidative/nitrosative damage [25, 45]. To screen for the preservation of therapeutic function following antibody humanization, a neutrophil infiltration assay for MPO activity and a BBB locomotor test were performed on a selection of the humanized anti-CD11d clones. Following an experimental clip compression injury at T4, rats were treated with one of the following monoclonal antibody preparations: human IgG4 isotype control, murine 217 L anti-CD11d, and the five humanized anti-CD11d variants (anti-CD11d-1, anti-CD11d-2, anti-CD11d-3, anti-CD11d-4, anti-CD11d-5) (Fig. 2A). Spinal lesion homogenates were collected and assayed for MPO activity as a surrogate marker of neutrophil infiltration (Fig. 2B). MPO activity was significantly reduced in anti-CD11d treated rats when compared to MPO activity in the isotype control–treated rats. Importantly, there was no significant difference in the MPO activity between the original murine 217 L–treated rats and the five humanized anti-CD11d variants (Fig. 2B). A locomotor assessment using the BBB open-field locomotor assessment [39] was then performed to determine behavioral recovery following SCI. Due to resource constraints, one humanized antibody was selected to screen for preserved functionality. The anti-CD11d-3 clone was chosen for use in the rat locomotor testing because it induced the greatest reduction in rat MPO levels among the humanized clones. SCI rats that received anti-CD11d-3 treatment had significantly higher BBB open-field locomotor scores than the IgG4 isotype control–treated rats (Fig. 2C). These results were very similar to our previous SCI reports performed with the mouse 217 L monoclonal antibody [2, 46] (Fig. 2C).

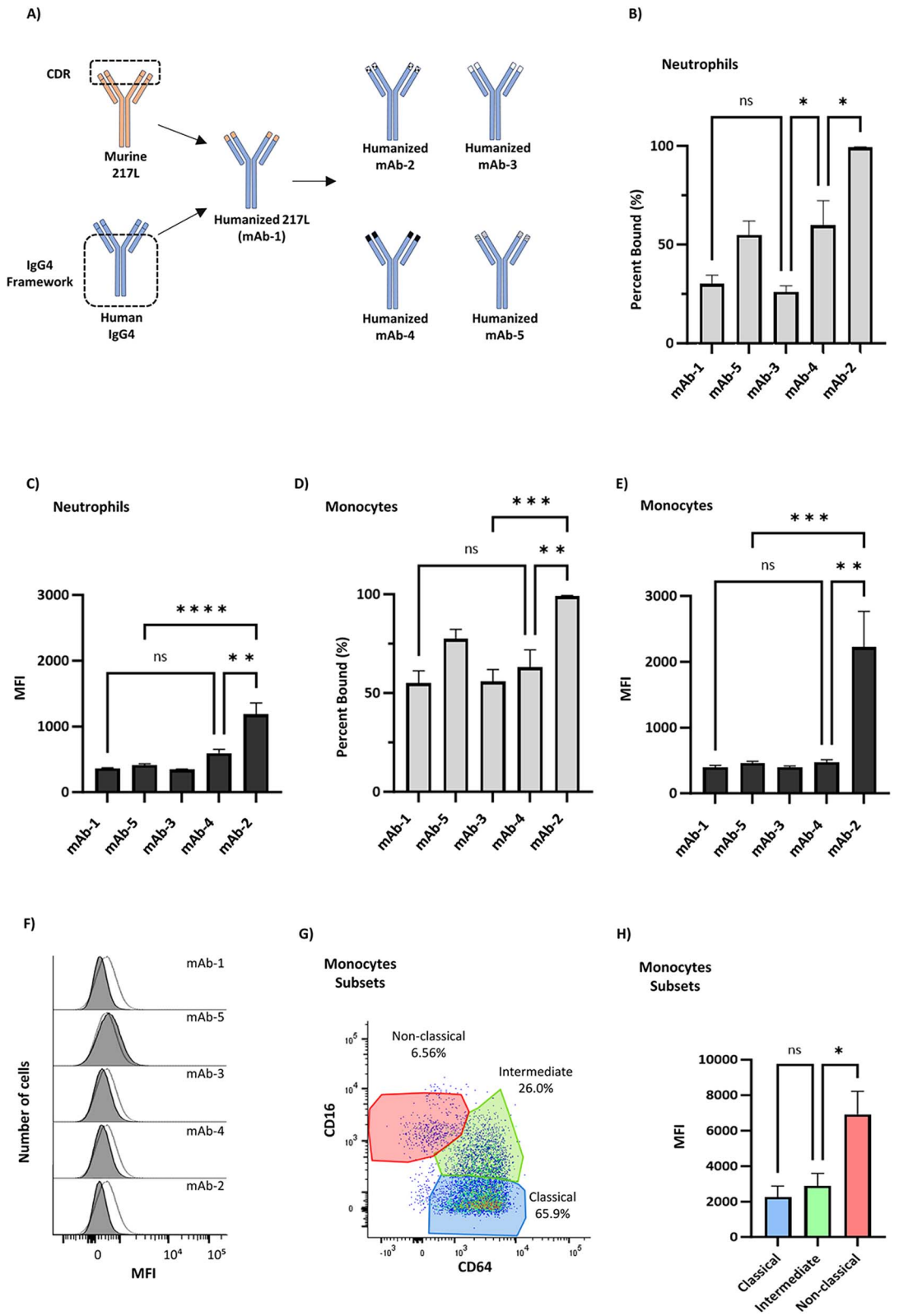

Figure 1. Creation of humanized anti-CD11d monoclonal antibodies. (A) Conceptual diagram of the components that were combined to create the humanized anti-CD11d clones. The murine 217 L clone CDR sequence was isolated and inserted into a human IgG4 framework. Four variants of the 217 L CDR sequence were subsequently made and inserted into the same human IgG4 framework. (B) Percent-bound and (C) quantified MFI flow cytometric analysis of anti-CD11d clone binding to primary human neutrophils ($N = 5$). (D) Percent-bound and (E) quantified MFI flow cytometric analysis of anti-CD11d antibodies binding to primary human monocytes. (F) Nonspecific binding of the anti-CD11d clones (shaded histogram) and IgG4 isotype control antibody (white histogram with black outline) to CD11d$^-$ Jurkat T cells. (G) Gating strategy identifying primary human monocyte subsets. (H) MFI analysis of CD11d expression among primary human monocyte subsets as determined by the humanized anti-CD11d-2 clone ($N = 4$). Error bars represent standard error. Significance was calculated by one-way ANOVA and Tukey's multiple comparisons test (*$P < .05$), (**$P < .01$), (***$P < .001$), and (****$P < .0001$).

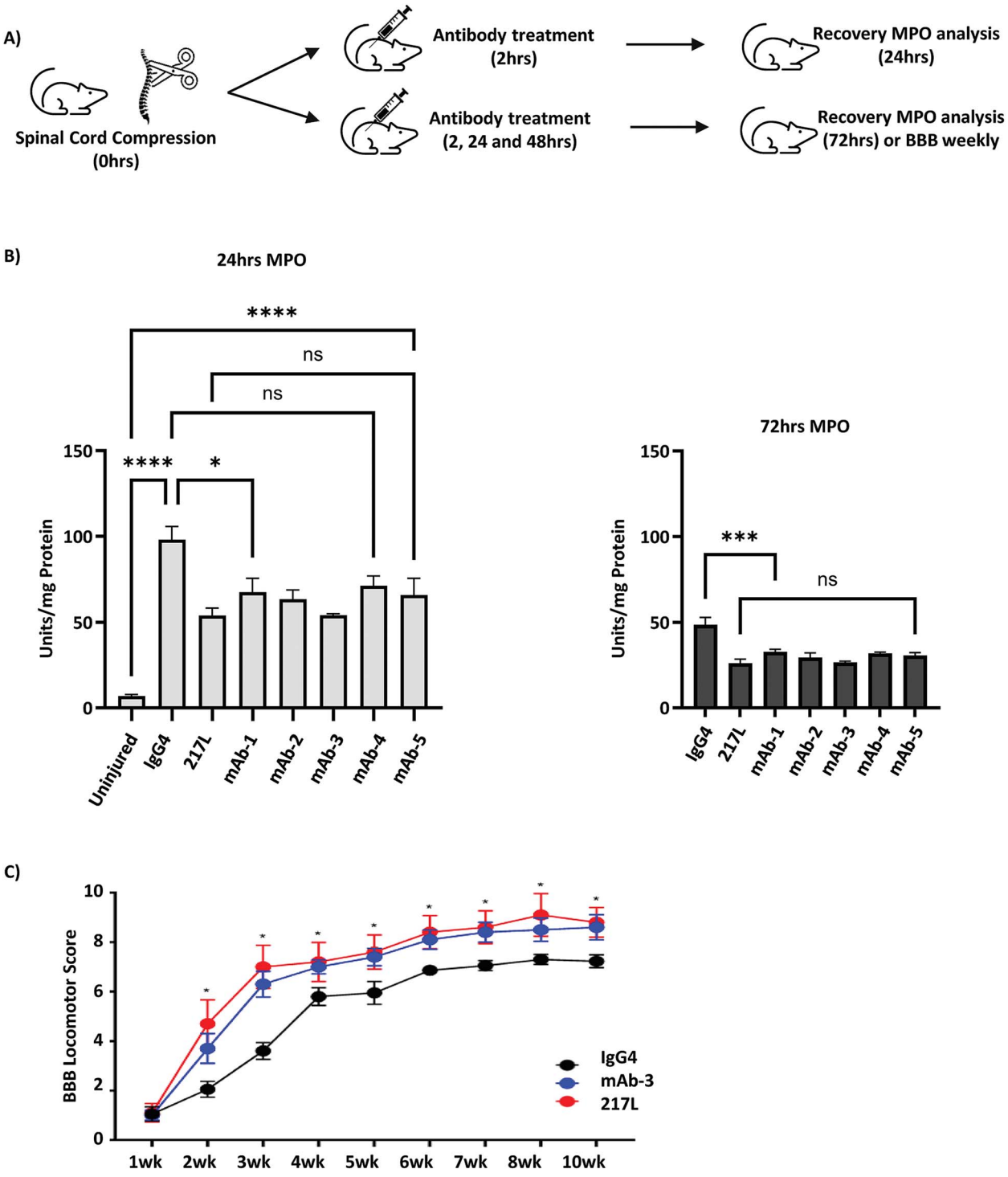

Figure 2. Humanized anti-CD11d clones improve biochemical and behavioral recovery in a rat SCI model. (A) Conceptual diagram of spinal cord compression injury and treatment with therapeutic anti-CD11d antibodies. (B) Spinal cord lesion homogenates from SCI rats treated with either anti-CD11d 1–5 or IgG4 isotype control antibody were assayed for myeloperoxidase as a surrogate for neutrophil infiltration ($N = 6$). Note an uninjured control was only performed for the 24-h timepoint. Error bars represent standard error. Significance was calculated by one-way ANOVA and Tukey's multiple comparisons test (*$P < .05$), (**$P < .01$), (***$P < .001$), (****$P < .0001$). (C) BBB open-field locomotor scores in anti-CD11d-3 treated rats ($N = 9$) and IgG4 isotype control-treated rats ($N = 10$). Error bars represent standard error. Two-way ANOVA and Newman–Keuls *post hoc* test demonstrated a significant treatment effect ($P = .0029$), a significant effect of time ($P < .0001$), and a significant interaction of treatment and time ($P = .0006$). The only time that is not significant is at 1 week when a difference is not expected. From 2 to 10 weeks, they are all significant at either $P < .01$ or $P < .05$. Note that there were no data obtained in week 9. This statistical analysis was performed on only the BBB scores from the anti-CD11d-3-treated and IgG4-treated rats. The 217 L–treated rats were a smaller group of rats added in to illustrate the degree of recovery was similar to the anti-CD11d-3-treated group.

Binding affinity of the humanized anti-CD11d-2 clone

The anti-CD11d-2 clone was determined to bind to the greatest percentage of human leukocytes (Fig. 1B) and thus we investigated its distinct binding dynamics. A THP-1 model was chosen to study the anti-CD11d binding dynamics because past genetic studies have demonstrated that PMA stimulation of THP-1 cells can dramatically increase the expression of CD11d mRNA [17]. Additional CD18 co-expression, however, is required for the transportation of functional CD11d/CD18 to the cell surface [18]. Flow cytometry was used to confirm upregulation of cell surface CD11d/CD18 expression following PMA differentiation of THP-1 cells (Fig. 3A). The increase in cell surface expression of CD11d/CD18 in PMA-differentiated THP-1 Luc2 cells was also verified with immunocytochemistry (Fig. 3B).

Establishing PMA-differentiated THP-1 cells as an endogenous CD11d/CD18 model permitted the characterization of anti-CD11d-2 binding affinity. The B_{max} for anti-CD11d-2 was found to be 85.5 ± 3.13% (mean ± SEM). The corresponding K_d was $3.55 \times 10^{-11} \pm 0.872 \times 10^{-11}$ M (mean ± SEM) (Fig. 3C). Treatment with Mn^{2+} forces the activate $\beta 2$ integrin conformation, whereas EDTA treatment forces the inactive confirmation [47, 48]. The binding dynamics of anti-CD11d-2 were not significantly different in the presence of Mn^{2+} or EDTA (Fig. 3C).

All the anti-CD11d antibodies in our study bind to the CD11d I-domain. The AlphaFold computational CD11d I-domain was analyzed to postulate anti-CD11d-2 epitope locations (Fig. 3D). A conserved $\alpha 7$-helix and a conserved negatively charged metal-ion-dependent adhesion site (MIDAS) motif were clearly visualized. The $\alpha 7$-helix, which elongates upon divalent cation binding to the MIDAS motif, was located opposite the proposed CD11d ligand binding site [1] (Fig. 3D).

No inflammatory signaling detected by the humanized anti-CD11d-2 clone

Upon binding, antibodies have the potential to act as a ligand and trigger a signaling cascade. We investigated the ability of anti-CD11d-2 to induce pro-inflammatory signaling upon binding CD11d/CD18 by evaluating Nuclear factor kappa B (NF-κB) expression in a THP-1 model system. First, both undifferentiated and differentiated THP-1 Luc2 cells activated a robust NF-κB response following lipopolysaccharide (LPS) treatment. Next, PMA-differentiated THP-1 Luc2 cells also induced NF-κB expression in response to VCAM-1 binding—a native CD11d ligand. Undifferentiated THP-1 cells, however, did not respond to VCAM-1 (Fig. 4A). Using VCAM-1 as a positive control, plates were then coated with anti-CD11d-2 or IgG4 isotype control antibodies. Differentiated Luc-2 THP-1 cells were subsequently added to the plates, and NF-κB expression was quantified over a 24-h period. No significant differences were found in peak NF-κB expression between all concentrations (1, 3, 5, and 10 μg/ml) of anti-CD11d-2, IgG4 isotype control, or empty untreated wells (Fig. 4B).

Outside-in integrin signaling via tyrosine phosphorylation was not observed following the binding of soluble anti-CD11d-2 to CD11d/CD18. Well-described $\beta 2$ integrin signaling consists of substantial tyrosine phosphorylation, including key signal transduction by FAK following ligand binding [49, 50]. Confluent layers of adherent PMA-differentiated THP-1 cells were stimulated with soluble anti-CD11d-2 or IgG4 isotype control antibody for 1 h. Western blot analysis then quantified general tyrosine phosphorylation and FAK phosphorylation at Tyr_{397}. No significant difference in tyrosine phosphorylation between anti-CD11d-2, IgG4 isotype control, or untreated wells was observed (Fig. 4C).

Inhibition of CK2 phosphorylation modulates $\beta 2$ integrin expression

Establishing anti-CD11d-2 as a refined total CD11d/CD18 detection tool allowed us to further investigate the unique expression profile of CD11d/CD18. A potential CD11d CK2 phosphorylation site—unique within the set of known $\beta 2$ integrins—is located on its terminal cytoplasmic tail [1]. We hypothesized that the prospective CD11d CK2 site may contribute to the unique CD11d expression profile. Using anti-CD11d-2 as a CD11d/CD18 detection reagent, we quantified $\beta 2$ integrin expression in a THP-1 model following PMA differentiation and CK2 inhibition. PMA differentiation upregulated $\beta 2$ integrin expression and caused the THP-1 cells to shift from CD11a dominance to CD11b-d dominance (Fig. 5). Next, CK2 phosphorylation in THP-1 cells was inhibited with a CGS-CK2-1 inhibitor [51] and verified by western blot analysis (Supplementary Fig. 1A). Unexpectedly, inhibiting CK2 phosphorylation during PMA differentiation downregulated general $\beta 2$ integrin expression but maintained the switch to CD11b-d dominance. A surface staining experiment was repeated with CK2 inhibition post-PMA differentiation, and the results were analogous (data not shown). Undifferentiated THP-1 cells were unaffected by CK2 inhibition (Fig. 5). The observed changes in $\beta 2$ expression were detected by combined cell surface and intracellular staining as determined by flow cytometry. Total cell $\beta 2$ integrin detection was decreased, indicating that protein expression was modulated, not integrin localization. CD18 expression was downregulated to levels observed in undifferentiated cells (Fig. 5). No difference in total vs surface level expression was observed in all the measured CD11 integrins except for CD11d, which did have a significantly higher level of total expression when compared to surface-level expression. Interestingly, the significant difference between total and surface-level expression of CD11d persisted with CK2 inhibition (Fig. 5).

Discussion

The development of humanized anti-CD11d monoclonal antibodies builds on more than two decades of *in vivo* research that details improvement by murine clones in recovery from neurotrauma in rodent models [2–5]. In a SCI rat model, the humanized anti-CD11d clones were screened and maintained their therapeutic benefit. Thus, at least from the perspective of preclinical animal data, the humanized recombinant CD11d monoclonal antibodies function *in vivo* as expected in comparison to our previously published data using murine monoclonal antibodies [2, 26].

Anti-CD11d-2 binds human CD11d/CD18 at the greatest percentage and MFI; therefore, we took a special interest in determining its binding dynamics. Performing additional binding dynamics in the presence of Mn^{2+} or EDTA provides evidence that anti-CD11d-2 binds CD11d regardless of integrin conformation (Fig. 3C). No crystallized CD11d structure is currently available for analysis. Instead, we used a predicted CD11d structure by AlphaFold to postulate on the anti-CD11d-2 epitope location (Fig. 3D). The $\alpha 7$-helix is known to elongate upon divalent cation binding [1, 52]. Given that anti-CD11d-2 binds regardless of the presence of divalent cations, we hypothesize that the anti-CD11d-2 epitope is located on the ligand binding surface opposite to the $\alpha 7$-helix. Promiscuous conformation binding allows anti-CD11d-2 to bind inactive and active CD11d/CD18 on peripheral blood leukocytes and active CD11d/CD18 on tissue-recruited

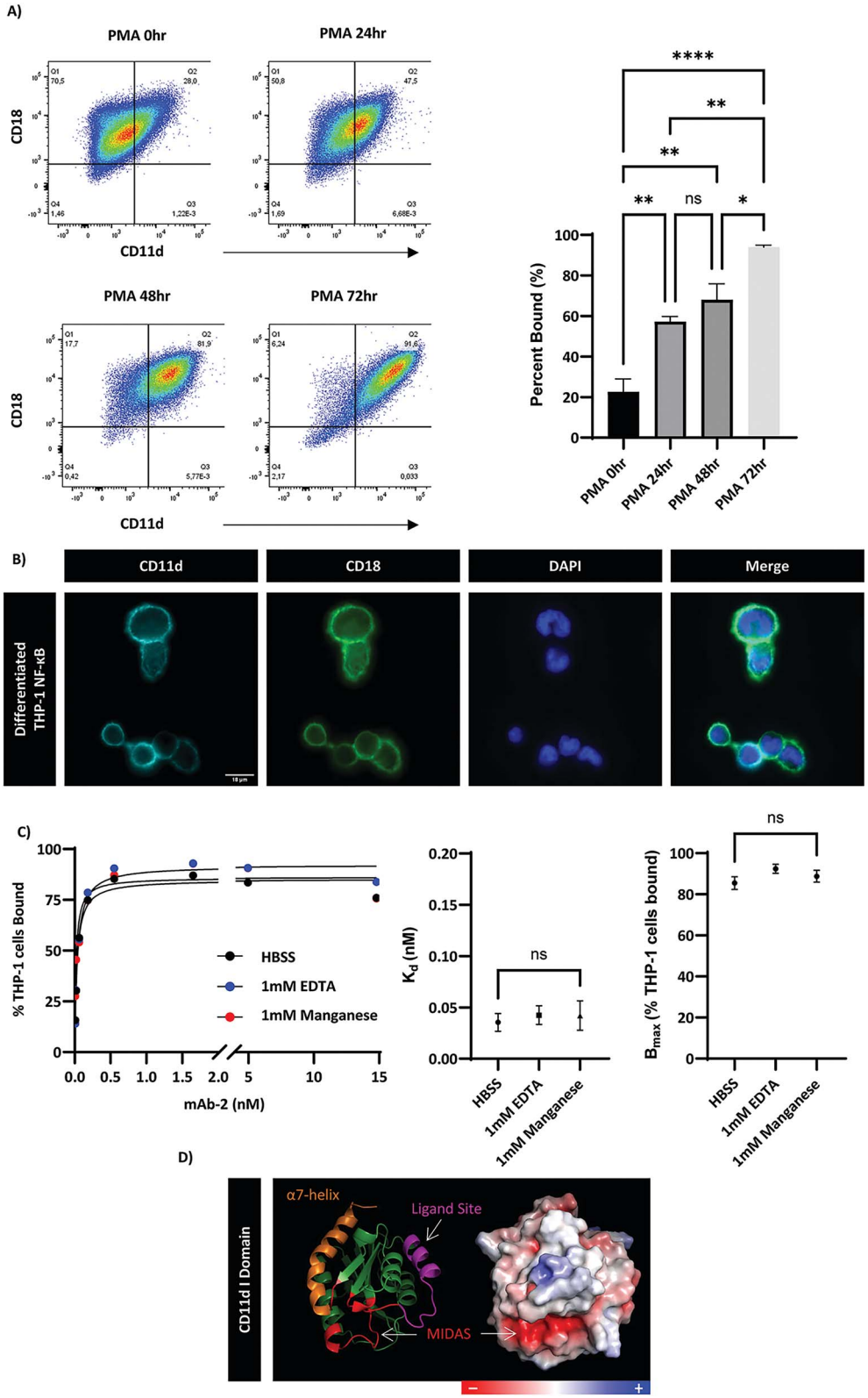

Figure 3. Humanized anti-CD11d-2 binding dynamics in a THP-1 model. (A) Flow cytometry analysis gated on live THP-1 cells differentiated with 100 nM PMA for up to 72 h ($N = 3$). (B) Immunohistochemistry of 100 nM PMA–differentiated THP-1 Luc2 cells for 72 h and then stained in the presence of human TruStain FcX block. Images are a representation of multiple fields of view ($n = 5$) across several independent repeats ($N = 3$). (C) Binding dynamics of anti-CD11d-2 to endogenous CD11d on 100 nM PMA–differentiated THP-1 cells as determined by flow cytometry ($N = 3$). Blocking and cell surface staining occurred live to allow for conformation change in HBSS, HBSS + 1 mM EDTA, or HBSS + 1 mM Mn^{2+}. Cells were subsequently fixed for analysis. The binding curve is presented using a break in the x-axis. Error bars represent standard error. Significance was calculated by one-way ANOVA and Tukey's multiple comparisons test (*$P < .05$), (**$P < .01$), (****$P < .0001$). (D) Predicted computational CD11d I-domain (residues 148–336) from AlphaFold (AF-Q13349-F1-v4). The ribbon diagram highlights the predicted α7-helix, MIDAS motif, and ligand binding site. The electrostatic diagram highlights the negatively charged MIDAS motif for divalent cation binding. Both the ribbon diagram and electrostatic diagram are of the same position in space.

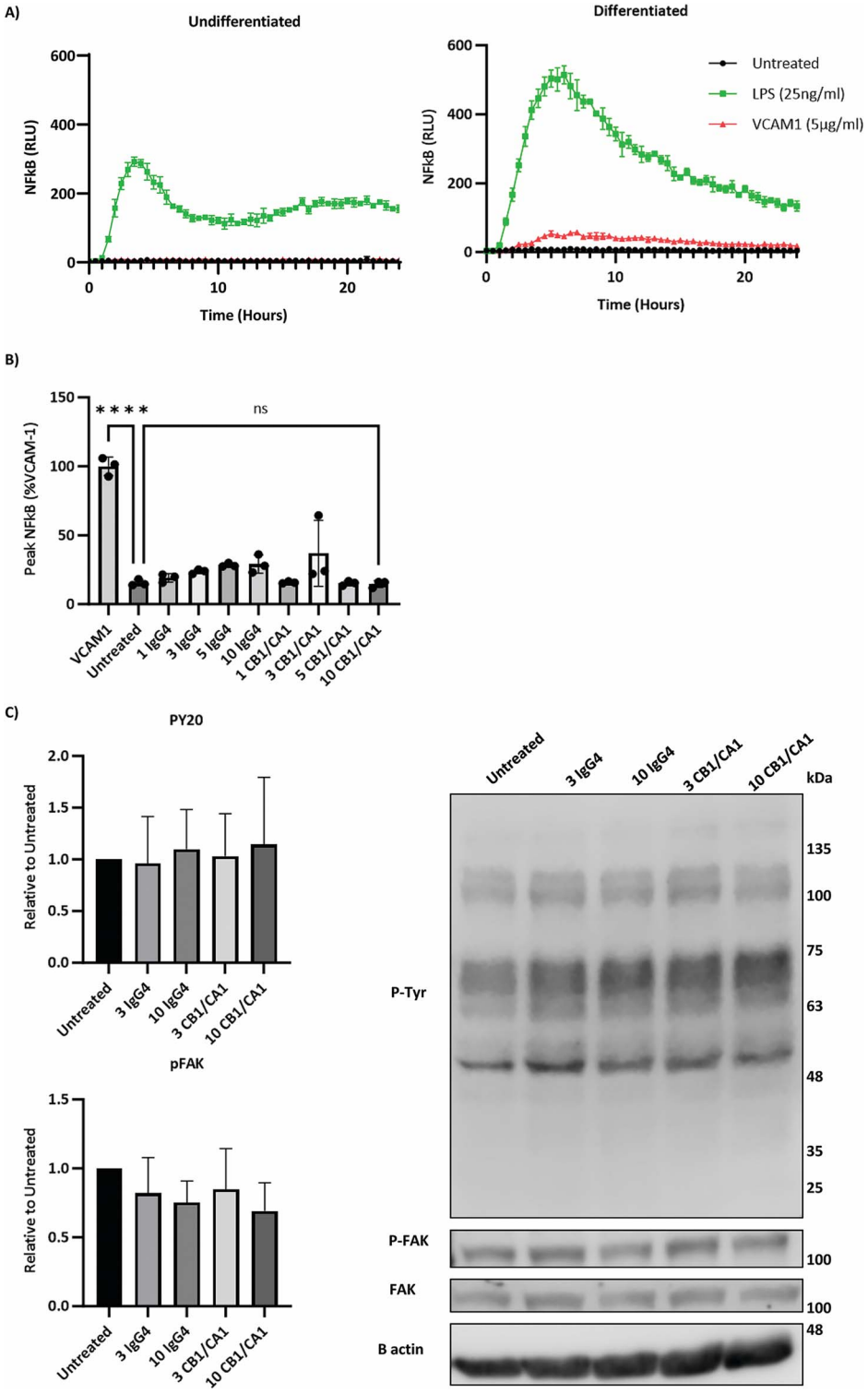

Figure 4. Absence of humanized anti-CD11d-2 inducing pro-inflammatory β2 integrin signaling. (A) NF-κB expression was detected by a luciferase assay in THP-1 Luc2 cells. Following a 48-h culture in the presence or absence of 100 nM PMA, THP-1 Luc2 cells were collected and blocked with 5% HSA. Blocked THP-1 Luc2 cells were dropped onto untreated wells, LPS (25 ng/ml) containing wells, or VCAM-1 (5 μg/ml) coated wells. The plates were incubated and NF-κB expression was measured in triplet every hour for 24 h ($N = 3$). (B) Luciferase NF-κB assay following anti-CD11d-2 stimulation in 4-h PMA differentiated THP-1 Luc2 cells. Cells blocked by 5% HSA were dropped onto plates coated with VCAM-1 (5 μg/ml) or various concentrations (μg/ml) of antibodies. The plates were incubated and NF-κB expression was measured in triplet every hour for 24 h ($N = 3$). Peak NF-κB expression was calculated as the mean value between 4- and 8-h poststimulation and normalized to VCAM-1 ($N = 3$). Significance was calculated by one-way ANOVA and Tukey's multiple comparisons test ($P < .05$), (****$P < .0001$). (C) Western blot analysis of 72-h 100 nM PMA–differentiated THP-1 cells stimulated with soluble anti-CD11d-2 (μg/ml) or IgG4 isotype control (μg/ml). Blots were performed in duplicate and normalized to untreated wells ($N = 3$). The representative images are from the same blot that was probed first for P-Tyr and FAK (Supplemental Fig. 3A), then re-probed for P-FAK and β-actin (Supplemental Fig. 3B). Monochrome cropped singlet rows of the same columns are displayed for each protein target. Error bars represent standard error. Significance was calculated by one-way ANOVA and Tukey's multiple comparisons test ($P < .05$).

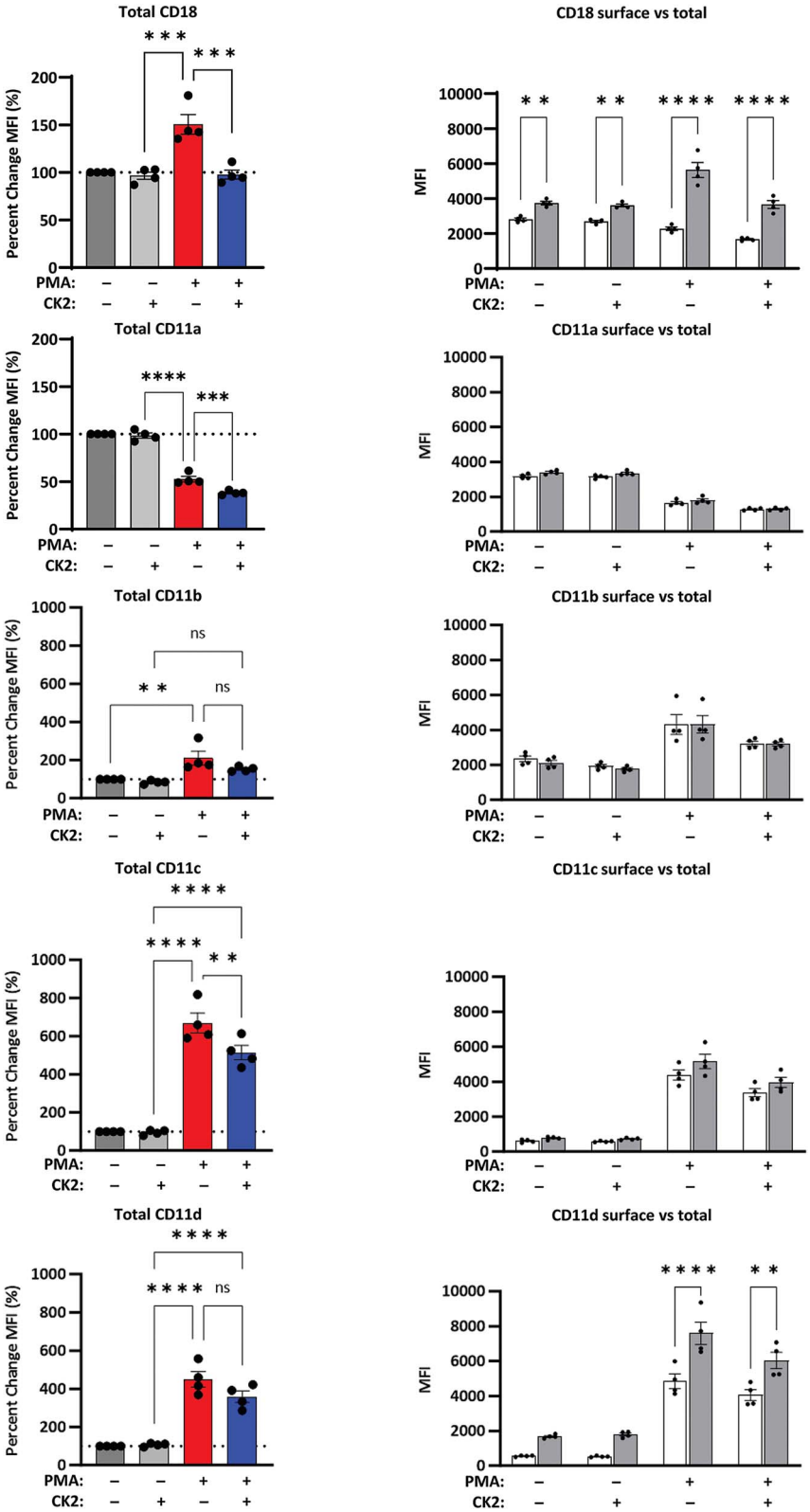

Figure 5. Modulation of $\beta 2$ integrin expression by CK2 inhibition. Flow cytometric analysis of $\beta 2$ integrin expression in THP-1 cells treated with combinations of 100 nM PMA and CGS-CK2-1 inhibitor (5 μg/ml) for 48 h. Surface level and internal level integrin expression were recorded to determine the surface level only (white) and total (grey) $\beta 2$ integrin expression. Error bars represent standard error, ($N = 3$). Significance between surface and total expression within a treatment group was calculated by a two-way ANOVA and Tukey's multiple comparisons (**$P < .01$), (***$P < .001$), (****$P < .0001$). Additional total $\beta 2$ integrin expression analysis was then performed between treatment groups. Error bars represent standard error, ($N = 3$). Significance in levels of total expression between treatment groups was calculated by one-way ANOVA and Tukey's multiple comparisons (**$P < .01$), (***$P < .001$), and (****$P < .0001$).

leukocytes. Differences in conformational binding activity may explain the observed differences in human peripheral blood leukocyte binding among the anti-CD11d clones and why anti-CD11d-2 binds the greatest percentage of cells (Fig. 1B).

The use of anti-CD11d-2 as a novel CD11d detection tool reinforces previous knowledge regarding the basal CD11d expression profile. The monoclonal and dual conformation binding nature of anti-CD11d-2 provides a refined tool for total CD11d detection. Consistent with the literature [1], we noted that both peripheral monocytes and neutrophils expressed CD11d/CD18 when detected by ant-CD11d-2. The level of CD11d/CD18 expression was consistently low across neutrophils and monocytes except for nonclassical $CD14^+CD16^+$ monocytes that expressed high levels of CD11d on the cells' surface. Nonclassical $CD14^+CD16^+$ monocytes were a small proportion of total monocytes, which explains why previous studies found the overall monocyte pool to express low levels of CD11d [8, 53]. The same previous studies were also divided regarding the level of CD11d expression on nonclassical $CD14^+CD16^+$ monocytes [8, 53]. Our data using the anti-CD11d-2 detection tool support the conclusion that nonclassical $CD14^+CD16^+$ monocytes express relatively greater CD11d levels [53] instead of lower levels of expression [8]. Resolving the conflicting data permits future investigation into the mechanism by which CD11d/CD18 may influence the unique role and migration patterns of nonclassical $CD14^+CD16^+$ monocytes.

We further investigated the dynamics of anti-CD11d-2 to determine if any inflammatory signaling was induced upon binding human CD11d/CD18. A previous study described the release of IL-8, IL-1β, and MCP-1 by THP-1 cells when exposed to plates coated with ICAM-3 or murine anti-CD11d clones [8]. To our knowledge, however, the mechanistic pathway for a CD11d/CD18 signaling cascade has not been described. In the absence of any literature on a known CD11d/CD18 outside-in signaling pathway, NF-κB expression and tyrosine phosphorylation were selected as broad measures of inflammatory signaling within a THP-1 cell model. Well-described β2 integrin signaling cascades involve tyrosine phosphorylation and can induce NF-κB expression [49, 50, 54]. Here we demonstrated that only differentiated THP-1 cells can induce NF-κB expression following VCAM-1 binding (Fig. 4A). Determining the contribution of CD11d/CD18 alone (which induces signaling upon binding VCAM-1) is limited by the multitude of integrins that may also bind VCAM-1. Of note, $\alpha4\beta1$ (VLA-4) interacts with VCAM-1 to contribute to the induction of NF-κB expression [55, 56]. Future studies may parse out the individual contributions of CD11d/CD18 interactions toward NF-κB expression and identify a CD11d/CD18 signaling cascade upon binding of VCAM-1. In the context of our current study, VCAM-1 served as a positive control for integrin-induced NF-κB expression to compare against the humanized anti-CD11d-2 clone on ligand-coated plates. Designed as an IgG4 antibody, anti-CD11d-2 did not induce a significant inflammatory response upon binding CD11d/CD18. There was an observed absence in NF-κB expression following plate-coated anti-CD11d-2 binding and no observed FAK outside-in signaling following soluble anti-CD11d-2 binding. Thus, in addition to being a refined detection tool for human CD11d/CD18, anti-CD11d-2 has the capacity to be pursued as an effective therapeutic antibody that blocks CD11d binding without inducing its own inflammatory signaling cascade.

CK2 inhibitors have long been known to modulate inflammatory responses [57]. Downregulation of all β2 integrins following CK2 inhibition, however, was an unexpected result (Fig. 5). The use of an analogous CK2 inhibitor (CX-4945) in glioblastoma cells was previously shown to downregulate the $\beta1$ and $\alpha4$ genes that form $\alpha4\beta1$ and $\alpha4\beta7$ integrins [58]. A proposed mechanism of integrin downregulation in glioblastoma cells was the inhibition of NF-κB activation [58]. Remodeling of β2 integrin expression by CK2 inhibition may result in functional changes to myeloid cell localization. A previous study found that CK2 knock-out mice have increased monocyte and neutrophil recruitment when infected with *Listeria monocytogenes* [59]. Integrin density is key in determining if a leukocyte will favor tissue migration or tissue retention. Adhesive forces are required for cell migration, but excessive adhesive forces induce cell immobility. Mathematic models have described the relationship between adhesive forces and cell mobility [60, 61], which are then observed in CD11d and CD11b models [62–64]. The partial downregulation of β2 integrins by CK2 inhibition may be sufficient to switch the adhesive forces from favoring cell immobility to cell migration. Future studies may investigate if CK2 inhibition can encourage leukocyte migration among pathophysiologies in which excessive CD11b/CD18 and/or CD11d/CD18 expression causes immobilization and harmful leukocyte accumulation. Future avenues also exist to determine the cause of the discrepancy between total and surface-level CD11d expression that was not resolved by the actions of CK2 phosphorylation.

The goal of anti-CD11d therapy is to modulate the waves of leukocytes that extravasate into target tissues through CD11d/CD18 and VCAM-1 interactions. Our laboratory has extensively investigated the validity of acute anti-CD11d therapy in rodent neurotrauma models [2–5]. Temporary use of a blocking clone can target and prevent the extravasation of initial pro-inflammatory leukocytes immediately following neurotrauma without affecting the subsequent recruitment of wound-healing leukocytes [65]. Looking beyond neurotrauma, CD11d blockade may also have a therapeutic role in acute inflammatory lung pathologies. The isolated deletion of CD11d alone can provide remarkable improvements in lung pathology and overall survival within a murine sepsis model [66]. Going beyond VCAM-1-mediated extravasation, anti-CD11d therapeutics have the potential to modulate tissue retention/migration mediated by CD11d/CD18 and extracellular matrix interactions. A small peptide inhibitor of CD11d interactions reduced macrophage retention in adipose tissue, which is observed in atherosclerosis and diabetes [6]. Indeed, $CD11d^{-/-}$ mice demonstrate a reduced disease burden in a murine atherosclerosis model [10]. Multiple avenues of investigation, therefore, exist to apply a temporary CD11d blockade with humanized anti-CD11d monoclonal antibodies and achieve a therapeutic goal.

Conclusion

In conclusion, we present five humanized anti-CD11d monoclonal antibodies. When screened, anti-CD11d-3 maintained its therapeutic functionality in a rodent neurotrauma model. A high affinity anti-CD11d-2 clone bound both conformations of CD11d/CD18 and did not produce an inflammatory response during *in vitro* assays. Anti-CD11d-2 was then used to detect a surprising pan-β2 integrin downregulation following inhibition of CK2 phosphorylation and a mismatch between total and surface-level CD11d expression. Future studies may use the humanized anti-CD11d clones as tools to propel CD11d/CD18 research when investigating the therapeutic role of CD11d/CD18 blockade in neurotrauma, sepsis, and atherosclerosis.

Supplementary data

Supplementary data are available at *ABT* online.

Acknowledgements

We thank Feng Bao, Todd Hryciw, Nicole Geremia, and Kevin Braden from the Robarts Research Institute at the University of Western Ontario laboratories of Drs Lynne C. Weaver, Arthur Brown, and Gregory Dekaban, respectively, for conducting important experiments in this report.

Author contributions

The concept for this paper was that of Gregory Dekaban with contributions from Lynne Weaver and Arthur Brown. The manuscript was written by Eoin N. Blythe and edited by Drs. Gregory Dekaban, Lynne Weaver, and Arthur Brown. Christy Barreira also contributed to the editing of the manuscript. Eoin Blythe (Conceptualization [supporting], Data curation, Formal analysis, Investigation, Methodology, Writing—review & editing [equal], Software, Writing—original draft [lead]), Christy Barreira (Formal analysis, Methodology [equal], Investigation, Resources, Writing—review & editing [supporting]), Corby Fink (Formal analysis, Methodology [equal], Writing—review & editing [supporting]), Arthur Brown (Conceptualization, Funding acquisition, Investigation, Methodology, Supervision [equal], Writing—review & editing [supporting]), Lynne Weaver (Conceptualization, Data curation, Formal analysis, Funding acquisition, Investigation, Methodology, Resources [equal], Writing—review & editing [supporting]), and Gregory Dekaban (Conceptualization, Funding acquisition, Investigation, Project administration, Supervision [lead], Formal analysis, Methodology, Writing—original draft, Writing—review & editing [equal]).

Conflict of interest

The authors share the following patents with Eli Lilly & Company:

Japanese Awarded Patent Number: 7328762
Patentees**:** The University of Western Ontario, 100 Colip Circle, Suite 105, Ontario N6G 4X8 Canada;
Inventors: Gregory Dekaban, Arthur Brown, Lynne Weaver.
Patentees: Eli Lilly and Company, Lilly Corporate Center, Indianapolis, Indiana 46285 U.S.A.
Inventors: Barrett Allan, Kristine Kikly.

United States Awarded Patent Number: US 11,873,340 B2
Patentees: The University of Western Ontario, 100 Colip Circle, Suite 105, Ontario N6G 4X8 Canada;
Inventors: Gregory Dekaban, Arthur Brown, Lynne Weaver.
Patentees: Eli Lilly and Company, Lilly Corporate Center, Indianapolis, Indiana 46285 U.S.A.
Inventors: Barrett Allan, Kristine Kikly.

Canadian Pending Patent Number:
Patentees: The University of Western Ontario, 100 Colip Circle, Suite 105, Ontario N6G 4X8 Canada.
Inventors**:** Gregory Dekaban, Arthur Brown, Lynne Weaver.
Patentees**:** Eli Lilly and Company, Lilly Corporate Center, Indianapolis, Indiana 46285 U.S.A.
Inventors: Barrett Allan, Kristine Kikly.

Funding

The research reported here was supported in part by the U.S. Department of Defense CDRMP SCIRP grant SC090328P, CIHR OPG 363209 and the National Hockey League Players Associate Concussion Challenge Fund. Eli Lilly and Company did not provide any direct funding to any of the authors of this manuscript. Eli Lilly supplied the antibodies that the authors report on in this manuscript, as an in-kind contribution to the development and functional characterization of the humanized anti-CD11d antibodies.

Data availability

Upon reasonable request, all data can be acquired by contacting the corresponding author.

Ethics and consent statement

Acquiring human blood samples for this study was approved (Project ID: 7332) by the University of Western Ontario Health Science Ethics Review Board (HSERB). After obtaining informed consent, human peripheral blood was collected as approved by the HSERB Project 7332 and in accordance with an approved University of Western Ontario Biosafety-Biohazard Protocol (BIO-RRI-0021).

Animal research statement

All animal experiments were approved by the University of Western Ontario's Animal Care Committee (AUP no. 2010–237) and conducted in accordance with the Canadian Council of Animal Care guidelines, the University Animal Care Committee's Standard Operating Procedures and in accordance with the University's Biosafety-Biohazard Protocol (BIO-RRI-0021). Additionally, all animal experiments were conducted in accordance with the Standards for Humane Care and Use of Laboratory Animals as approved by the Office of Laboratory Animal Welfare, Department of Health & Human Services, U.S.A. (Protocol Assurance Identification #A5527-01). The studies reported were conducted in a manner consistent with ARRIVE guidelines.

References

1. Blythe EN, Weaver LC, Brown A. *et al.* β2 integrin CD11d/CD18: from expression to an emerging role in staged leukocyte migration. *Front Immunol* 2021;**12**:4471. https://doi.org/10.3389/fimmu.2021.775447.
2. Gris D, Marsh DR, Oatway MA. *et al.* Transient blockade of the CD11d/CD18 integrin reduces secondary damage after spinal cord injury, improving sensory, autonomic, and motor function. *J Neurosci* 2004;**24**:4043–51. https://doi.org/10.1523/JNEUROSCI.5343-03.2004.
3. Geremia NM, Bao F, Rosenzweig TE. *et al.* CD11d antibody treatment improves recovery in spinal cord-injured mice. *J Neurotrauma* 2012;**29**:539–50. https://doi.org/10.1089/neu.2011.1976.
4. Utagawa A, Bramlett HM, Daniels L. *et al.* Transient blockage of the CD11d/CD18 integrin reduces contusion volume and macrophage infiltration after traumatic brain injury in rats. *Brain Res* 2008;**1207**:155–63. https://doi.org/10.1016/j.brainres.2008.02.057.
5. Shultz SR, Bao F, Weaver LC. *et al.* Treatment with an anti-CD11d integrin antibody reduces neuroinflammation and improves outcome in a rat model of repeated concussion. *J Neuroinflammation* 2013;**10**:26. https://doi.org/10.1186/1742-2094-10-26.
6. Cui K, Podolnikova NP, Bailey W. *et al.* Inhibition of integrin αDβ2–mediated macrophage adhesion to end product of docosahexaenoic acid (DHA) oxidation prevents macrophage accumulation during inflammation. *J Biol Chem* 2019;**294**:14370–82. https://doi.org/10.1074/jbc.RA119.009590.

7. Bao F, Bailey CS, Gurr KR. *et al.* Human spinal cord injury causes specific increases in surface expression of β integrins on leukocytes. *J Neurotrauma* 2011;**28**:269–80. https://doi.org/10.1089/neu.2010.1618.
8. Miyazaki Y, Vieira-de-Abreu A, Harris ES. *et al.* Integrin $\alpha D\beta 2$ (CD11d/CD18) is expressed by human circulating and tissue myeloid leukocytes and mediates inflammatory signaling. *PLoS One* 2014;**9**:1–25. https://doi.org/10.1371/journal.pone.0112770.
9. Shanley TP, Warner RL, Crouch LD. *et al.* Requirements for alpha d in IgG immune complex-induced rat lung injury. *J Immunol* 1998;**160**:1014–20. https://doi.org/10.4049/jimmunol.160.2.1014.
10. Aziz MH, Cui K, Das M. *et al.* The upregulation of integrin $\alpha D\beta 2$ (CD11d/CD18) on inflammatory macrophages promotes macrophage retention in vascular lesions and development of atherosclerosis. *J Immunol* 2017;**198**:4855–67. https://doi.org/10.4049/jimmunol.1602175.
11. Thomas AP, Dunn TN, Oort PJ. *et al.* Inflammatory phenotyping identifies CD11d as a gene markedly induced in white adipose tissue in obese rodents and women. *J Nutr* 2011;**141**:1172–80. https://doi.org/10.3945/jn.110.127068.
12. Shen Z, Shen B, Dai W. *et al.* Expansion of macrophage and liver sinusoidal endothelial cell subpopulations during non-alcoholic steatohepatitis progression. *iScience* 2023;**26**:1–19. https://doi.org/10.1016/j.isci.2023.106572.
13. Koelsch N, Mirshahi F, Aqbi HF. *et al.* The crosstalking immune cells network creates a collective function beyond the function of each cellular constituent during the progression of hepatocellular carcinoma. *Sci Rep* 2023;**13**:12630. https://doi.org/10.1038/s41598-023-39020-w.
14. Noti JD, Johnson AK, Dillon JD. Structural and functional characterization of the leukocyte integrin gene CD11d: ESSENTIAL ROLE OF Sp1 AND Sp3*. *J Biol Chem* 2000;**275**:8959–69. https://doi.org/10.1074/jbc.275.12.8959.
15. Noti JD. Expression of the myeloid-specific leukocyte integrin gene CD11d during macrophage foam cell differentiation and exposure to lipoproteins. *Int J Mol Med* 2002;**10**:721–7. https://doi.org/10.3892/ijmm.10.6.721.
16. Noti JD, Johnson AK, Dillon JD. The zinc finger transcription factor transforming growth factor beta-inducible early gene-1 confers myeloid-specific activation of the leukocyte integrin CD11d promoter. *J Biol Chem* 2004;**279**:26948–58. https://doi.org/10.1074/jbc.M310634200.
17. Noti JD, Johnson AK, Dillon JD. The leukocyte integrin gene CD11d is repressed by gut-enriched Kruppel-like factor 4 in myeloid cells. *J Biol Chem* 2005;**280**:3449–57. https://doi.org/10.1074/jbc.M412627200.
18. McKillop WM, Barrett JW, Pasternak SH. *et al.* The extracellular domain of CD11d regulates its cell surface expression. *J Leukoc Biol* 2009;**86**:851–62. https://doi.org/10.1189/jlb.0309150.
19. Schwab N, Ulzheimer JC, Fox RJ. *et al.* Fatal PML associated with efalizumab therapy: insights into integrin $\alpha L\beta 2$ in JC virus control. *Neurology* 2012;**78**:458–67. https://doi.org/10.1212/WNL.0b013e3182478d4b.
20. DeNucci CC, Pagan AJ, Mitchell JS. *et al.* Control of $\alpha 4\beta 7$ integrin expression and CD4 t cell homing by the $\beta 1$ integrin subunit. *J Immunol* 2010;**184**:2458–67. https://doi.org/10.4049/jimmunol.0902407.
21. Schneider I, Allner C, Mühl L. *et al.* Expression and function of $\alpha 4\beta 7$ integrin predict the success of vedolizumab treatment in inflammatory bowel disease. *Transl Res* 2023;**253**:8–15. https://doi.org/10.1016/j.trsl.2022.10.003.
22. Qiu B, Liang J-X, Li C. Efficacy and safety of vedolizumab for inflammatory bowel diseases: a systematic review and meta-analysis of randomized controlled trials. *Medicine (Baltimore)*. 2022;**101**:e30590. https://doi.org/10.1097/MD.0000000000030590.
23. Ha C, Kornbluth A. Vedolizumab as a treatment for Crohn's disease and ulcerative colitis. *Gastroenterol Hepatol (N Y)* 2014;**10**:793–800.
24. Mabon PJ, Weaver LC, Dekaban GA. Inhibition of monocyte/-macrophage migration to a spinal cord injury site by an antibody to the integrin alphaD: a potential new anti-inflammatory treatment. *Exp Neurol* 2000;**166**:52–64. https://doi.org/10.1006/exnr.2000.7488.
25. Bao F, Chen Y, Dekaban GA. *et al.* Early anti-inflammatory treatment reduces lipid peroxidation and protein nitration after spinal cord injury in rats. *J Neurochem* 2004;**88**:1335–44. https://doi.org/10.1046/j.1471-4159.2003.02240.x.
26. Saville LR, Pospisil CH, Mawhinney LA. *et al.* A monoclonal antibody to CD11d reduces the inflammatory infiltrate into the injured spinal cord: a potential neuroprotective treatment. *J Neuroimmunol* 2004;**156**:42–57. https://doi.org/10.1016/j.jneuroim.2004.07.002.
27. Oatway MA, Chen Y, Bruce JC. *et al.* Anti-CD11d integrin antibody treatment restores normal serotonergic projections to the dorsal, intermediate, and ventral horns of the injured spinal cord. *J Neurosci* 2005;**25**:637–47. https://doi.org/10.1523/JNEUROSCI.3960-04.2005.
28. Gris D, Marsh DR, Dekaban GA. *et al.* Comparison of effects of methylprednisolone and anti-CD11d antibody treatments on autonomic dysreflexia after spinal cord injury. *Exp Neurol* 2005;**194**:541–9. https://doi.org/10.1016/j.expneurol.2005.03.016.
29. Bao F, Chen Y, Dekaban GA. *et al.* An anti-CD11d integrin antibody reduces cyclooxygenase-2 expression and protein and DNA oxidation after spinal cord injury in rats. *J Neurochem* 2004;**90**:1194–204. https://doi.org/10.1111/j.1471-4159.2004.02580.x.
30. Weaver LC, Bao F, Dekaban GA. *et al.* CD11d integrin blockade reduces the systemic inflammatory response syndrome after traumatic brain injury in rats. *Exp Neurol* 2015;**271**:409–22. https://doi.org/10.1016/j.expneurol.2015.07.003.
31. Bao F, Brown A, Dekaban GA. *et al.* CD11d integrin blockade reduces the systemic inflammatory response syndrome after spinal cord injury. *Exp Neurol* 2011;**231**:272–83. https://doi.org/10.1016/j.expneurol.2011.07.001.
32. Gris P, Tighe A, Thawer S. *et al.* Gene expression profiling in anti-CD11d mAb-treated spinal cord-injured rats. *J Neuroimmunol* 2009;**209**:104–13. https://doi.org/10.1016/j.jneuroim.2009.02.002.
33. Bao F, Bailey CS, Gurr KR. *et al.* Increased oxidative activity in human blood neutrophils and monocytes after spinal cord injury. *Exp Neurol* 2009;**215**:308–16. https://doi.org/10.1016/j.expneurol.2008.10.022.
34. Grayson MH, Van der Vieren M, Sterbinsky SA. *et al.* alphadbeta2 integrin is expressed on human eosinophils and functions as an alternative ligand for vascular cell adhesion molecule 1 (VCAM-1). *J Exp Med* 1998;**188**:2187–91. https://doi.org/10.1084/jem.188.11.2187.
35. Dekaban, Gregory. *et al.*, inventors; The University of Western Ontario, Eli Lilly and Company, assignees; Anti-CD11D Antibodies and Uses Thereof. United States patent US 11873340. 2024.
36. Fink C, Smith M, Gaudet JM. *et al.* Fluorine-19 cellular MRI detection of in vivo dendritic cell migration and subsequent induction of tumor antigen-specific immunotherapeutic response. *Mol Imaging Biol* 2020;**22**:549–61. https://doi.org/10.1007/s11307-019-01393-8.
37. *FlowJo™ Software mac, v10.8*. BD Biosciences.

38. Weaver LC, Verghese P, Bruce JC. *et al.* Autonomic dysreflexia and primary afferent sprouting after clip-compression injury of the rat spinal cord. *J Neurotrauma* 2001;**18**:1107–19. https://doi.org/10.1089/08977150152693782.
39. Basso DM, Beattie MS, Bresnahan JC. A sensitive and reliable locomotor rating scale for open field testing in rats. *J Neurotrauma* 1995;**12**:1–21. https://doi.org/10.1089/neu.1995.12.1.
40. Fiji: an open-source platform for biological-image analysis. *Nat Methods* 2012;**7**:676–82. https://doi.org/10.1038/nmeth.2019.
41. Wells CI, Drewry DH, Pickett JE. *et al.* Development of a potent and selective chemical probe for the pleiotropic kinase CK2. *Cell Chem Biol* 2021;**28**:546–558.e10. https://doi.org/10.1016/j.chembiol.2020.12.013.
42. Varadi M, Bertoni D, Magana P. *et al.* AlphaFold protein structure database in 2024: providing structure coverage for over 214 million protein sequences. *Nucleic Acids Res* 2024;**52**:D368–75. https://doi.org/10.1093/nar/gkad1011.
43. Jumper J, Evans R, Pritzel A. *et al.* Highly accurate protein structure prediction with AlphaFold. *Nature* 2021;**596**:583–9. https://doi.org/10.1038/s41586-021-03819-2.
44. Siegers GM, Barreira CR, Postovit L-M. *et al.* CD11d β2 integrin expression on human NK, B, and $\gamma\delta$ T cells. *J Leukoc Biol* 2017;**101**:1029–35. https://doi.org/10.1189/jlb.3AB0716-326RR.
45. Bao F, Dekaban GA, Weaver LC. Anti-CD11d antibody treatment reduces free radical formation and cell death in the injured spinal cord of rats. *J Neurochem* 2005;**94**:1361–73. https://doi.org/10.1111/j.1471-4159.2005.03280.x.
46. Weaver LC, Gris D, Saville LR. *et al.* Methylprednisolone causes minimal improvement after spinal cord injury in rats, contrasting with benefits of an anti-integrin treatment. *J Neurotrauma* 2005;**22**:1375–87. https://doi.org/10.1089/neu.2005.22.1375.
47. Ye F, Kim C, Ginsberg MH. Reconstruction of integrin activation. *Blood* 2012;**119**:26–33. https://doi.org/10.1182/blood-2011-04-292128.
48. Zhang K, Chen J. The regulation of integrin function by divalent cations. *Cell Adhes Migr* 2012;**6**:20–9. https://doi.org/10.4161/cam.18702.
49. Hogg N, Patzak I, Willenbrock F. The insider's guide to leukocyte integrin signalling and function. *Nat Rev Immunol* 2011;**11**:416–26. https://doi.org/10.1038/nri2986.
50. Chang Y-C, Su W, Cho E. *et al.* Molecular basis for autoinhibition of RIAM regulated by FAK in integrin activation. *Proc Natl Acad Sci USA* 2019;**116**:3524–9. https://doi.org/10.1073/pnas.1818880116.
51. Menyhart D, Gyenis L, Jurcic K. *et al.* Comparison of CX-4945 and SGC-CK2-1 as inhibitors of CSNK2 using quantitative phosphoproteomics: triple SILAC in combination with inhibitor-resistant CSNK2. *Curr Res Chem Biol* 2023;**3**:100041. https://doi.org/10.1016/j.crchbi.2023.100041.
52. Xiong J-P, Li R, Essafi M. *et al.* An isoleucine-based allosteric switch controls affinity and shape shifting in integrin CD11b A-domain*. *J Biol Chem* 2000;**275**:38762–7. https://doi.org/10.1074/jbc.C000563200.
53. Steppich B, Dayyani F, Gruber R. *et al.* Selective mobilization of CD14(+)CD16(+) monocytes by exercise. *Am J Physiol Cell Physiol* 2000;**279**:C578–86. https://doi.org/10.1152/ajpcell.2000.279.3.C578.
54. Kim CH, Lee K-H, Lee C-T. *et al.* Aggregation of beta2 integrins activates human neutrophils through the IkappaB/NF-kappaB pathway. *J Leukoc Biol* 2004;**75**:286–92. https://doi.org/10.1189/jlb.0103038.
55. Mussbacher M, Salzmann M, Brostjan C. *et al.* Cell type-specific roles of NF-κB linking inflammation and thrombosis. *Front Immunol* 2019;**10**:85. https://doi.org/10.3389/fimmu.2019.00085.
56. Kong D-H, Kim YK, Kim MR. *et al.* Emerging roles of vascular cell adhesion Molecule-1 (VCAM-1) in immunological disorders and cancer. *Int J Mol Sci* 2018;**19**:1057. https://doi.org/10.3390/ijms19041057.
57. Hong H, Benveniste EN. The immune regulatory role of protein kinase CK2 and its implications for treatment of cancer. *Biomedicine* 2021;**9**:1932. https://doi.org/10.3390/biomedicines9121932.
58. Zheng Y, McFarland BC, Drygin D. *et al.* Targeting protein kinase CK2 suppresses Prosurvival Signaling pathways and growth of glioblastoma. *Clin Cancer Res* 2013;**19**:6484–94. https://doi.org/10.1158/1078-0432.CCR-13-0265.
59. Larson SR, Bortell N, Illies A. *et al.* Myeloid cell CK2 regulates inflammation and resistance to bacterial infection. *Front Immunol* 2020;**11**:1–19. https://doi.org/10.3389/fimmu.2020.590266.
60. DiMilla PA, Barbee K, Lauffenburger DA. Mathematical model for the effects of adhesion and mechanics on cell migration speed. *Biophys J* 1991;**60**:15–37. https://doi.org/10.1016/S0006-3495(91)82027-6.
61. Palecek SP, Loftus JC, Ginsberg MH. *et al.* Integrin-ligand binding properties govern cell migration speed through cell-substratum adhesiveness. *Nature* 1997;**385**:537–40. https://doi.org/10.1038/385537a0.
62. Yakubenko VP, Belevych N, Mishchuk D. *et al.* The role of integrin αDβ2 (CD11d/CD18) in monocyte/macrophage migration. *Exp Cell Res* 2008;**314**:2569–78. https://doi.org/10.1016/j.yexcr.2008.05.016.
63. Lishko VK, Yakubenko VP, Ugarova TP. The interplay between integrins alphaMbeta2 and alpha5beta1 during cell migration to fibronectin. *Exp Cell Res* 2003;**283**:116–26. https://doi.org/10.1016/S0014-4827(02)00024-1.
64. Cui K, Ardell CL, Podolnikova NP. *et al.* Distinct migratory properties of M1, M2, and resident macrophages are regulated by αDβ2 and αMβ2 integrin-mediated adhesion. *Front Immunol* 2018;**9**:2650. https://doi.org/10.3389/fimmu.2018.02650.
65. Thawer SG, Mawhinney L, Chadwick K. *et al.* Temporal changes in monocyte and macrophage subsets and microglial macrophages following spinal cord injury in the lys-egfp-ki mouse model. *J Neuroimmunol* 2013;**261**:7–20. https://doi.org/10.1016/j.jneuroim.2013.04.008.
66. Koutsogiannaki S, Hou L, Okuno T. *et al.* αDβ2 as a novel target of experimental polymicrobial sepsis. *Front Immunol* 2022;**13**:1–12. https://doi.org/10.3389/fimmu.2022.1059996.

Antibody Therapeutics, 2025, 8(1), tbae031
https://doi.org/10.1093/abt/tbae031
Research Article